Analytical study of a circular inhomogeneity with homogeneously imperfect interface in plane micropolar elasticity

J. Videla, E. Atroshchenko[1]

Department of Mechanical Engineering, University of Chile, Santiago, Chile

Abstract. In this paper we derive the full analytical solution for the problem of a circular micropolar inhomogeneity in an infinite micropolar plate subjected to a remote uni-axial tension. The interface between the inhomogeneity and the surrounding matrix is considered to be homogeneously imperfect, i.e. it is assumed that across the interface the stresses/couple stresses are continuous and proportional to the jumps in the corresponding displacements/microrotation. The solution method is based on the use of Eringen's stress functions, which allow to express all stresses/couple stresses and displacements/microrotation as a linear combination of the solutions of two governing equations and reduce the boundary conditions on the interface to a system of algebraic equations for the unknown coefficients.
A parametric study is conducted to show that the stress concentration factors are significantly dependent on the micropolar material constants as well as the parameters characterizing the imperfect bonding between the inclusion and the matrix.
The solution is given in a ready-to-use form, freely downloadable, and can be further used, for example, for the analysis of interface failures or as a reference solution in numerical methods.

Keywords. micropolar elasticity, inhomogeneity (inclusion), homogeneously imperfect interface.

1 Introduction

Micropolar elasticity is one of the generalized continuum theories, which was developed by the Cosserat brothers [1], Eringen [2], [3], Nowacki [4] and others to incorporate the effects of material microstructure directly into the constitutive equations. According to the provisions of the theory, the material is represented as a continuum of points, having both translational and rotational degrees of freedom. The applied loading creates a force and a couple, acting on every infinitesimal material plane, which leads to the description of the deformation in terms of the asymmetric stress and couple-stress tensors.

The theory introduces an intrinsic material length scale, associated with the material microstructure, which makes it suitable to model materials such as fibre-reinforced composites, granular and porous, blocky and layered materials. The theory is particularly adapted to describe materials with periodic microstructures, for which various homogenisation techniques have been developed for determination of material param-

[1]Corresponding Author, email: eatroshchenko@ing.uchile.cl, eatroshch@gmail.com

eters [5], [6]. For the materials with random microstructure, the material constants are measured experimentally, see for example, Lakes [7], [8].

A number of analytical and numerical methods have been proposed to solve the boundary value problems of micropolar elasticity: e.g. the finite element method [9], [10], [11]; the boundary element method for both, singular and hypersingular boundary integral equations was developed in [12], [13].

The accuracy of the numerical methods is usually assessed by comparison of the numerical results with the analytical solutions.

A common approach to obtain analytical solutions in the plane strain case is the generalisation of the Airy stress function method in classical elasticity, i.e. the stresses and couple stresses are expressed by means of two potential functions, introduced in [3], in the form of a series with the unknown coefficients determined from the boundary conditions. In [14] the analytical solutions for a number of problems were derived by the direct series expansion of the displacements and microrotations.

In this work we use the method of potential functions to develop the analytical solution for a problem of a micropolar circular inhomogeneity (inclusion) embedded into an infinite micropolar matrix subjected to a remote uni-axial tension. A problem with the same geometry and loading conditions was solved in [15] and [16] for the case of a micropolar elasticity with constrained rotations, known as couple-stress theory.

The bonding between the inclusion and the matrix in [15] and [16] was assumed to be perfect, i.e. the displacements, tractions and couple-tractions remain continuous across the interface. In the present work, we consider the more general case of a *homogeneously imperfect interface*, characterized by the continuous tractions and the jump in displacements proportional to the corresponding traction components. This model for plane elasticity was introduced in the work of Achenbach and Zhu [17], Hashin [18], [19], followed by the work of Bigoni [20], and further developed and generalized in [21], [22], [23] and others.

In this paper we generalise the model of a homogeneously imperfect interface to the case of micropolar elasticity, which is characterized by the additional conditions of continuous couple-traction and the jump in the microrotations proportional to the couple-traction. The dependence of the solutions on the micropolar material parameters as well as the parameters characterising the bond between the inhomogeneity and the matrix is analysed. Two limiting cases are also studied in details: a) strongly micropolar inclusion embedded in a matrix, described by classical elasticity and b) inclusion described by classical elasticity embedded in a strongly micropolar matrix.

While the paper contains the numerical results for some particular cases of the material and interface parameters, used for analysis, the full solution is provided in [24], in the form of Mathematica files, freely downloadable.

2 Preliminaries

For a micropolar material characterized by constants G (shear modulus), ν (Poisson's ratio), ℓ (characteristic length) and N (coupling number), the state of plane strain is described in polar coordinates by two displacements $u = u_r$, $v = u_\theta$, one out-of-plane microrotation $\phi = \phi_z$, stress tensor components σ_{rr}, $\sigma_{r\theta}$, $\sigma_{\theta r}$, $\sigma_{\theta\theta}$ and two couple stresses m_{rz}, $m_{\theta z}$. In [3] it has been shown that stresses and couple stresses can be

expressed in terms of two stress potentials Φ and Ψ, satisfying the equations:

$$\nabla^4\Phi = 0, \quad \nabla^2(c^2\nabla^2\Psi - \Psi) = 0 \tag{1}$$

together with the compatibility conditions:

$$\begin{aligned} \frac{\partial}{\partial r}(\Psi - c^2\nabla^2\Psi) &= -2(1-\nu)\ell^2\frac{1}{r}\frac{\partial}{\partial\theta}(\nabla^2\Phi), \\ \frac{1}{r}\frac{\partial}{\partial\theta}(\Psi - c^2\nabla^2\Psi) &= (1-\nu)\ell^2\frac{\partial}{\partial r}(\nabla^2\Phi), \end{aligned} \tag{2}$$

where $c = \dfrac{\ell}{N}$.

The stress and couple stress components are expressed as [3]:

$$\begin{aligned} \sigma_{rr} &= \frac{1}{r}\frac{\partial\Phi}{\partial r} + \frac{1}{r^2}\frac{\partial^2\Phi}{\partial\theta^2} - \frac{1}{r}\frac{\partial^2\Psi}{\partial r\partial\theta} + \frac{1}{r^2}\frac{\partial\Psi}{\partial\theta}, \\ \sigma_{\theta\theta} &= \frac{\partial^2\Phi}{\partial r^2} + \frac{1}{r}\frac{\partial^2\Psi}{\partial r\partial\theta} - \frac{1}{r^2}\frac{\partial\Psi}{\partial\theta}, \\ \sigma_{r\theta} &= -\frac{1}{r}\frac{\partial^2\Phi}{\partial r\partial\theta} + \frac{1}{r^2}\frac{\partial\Phi}{\partial\theta} - \frac{1}{r}\frac{\partial\Psi}{\partial r} - \frac{1}{r^2}\frac{\partial^2\Psi}{\partial\theta^2}, \\ \sigma_{\theta r} &= -\frac{1}{r}\frac{\partial^2\Phi}{\partial r\partial\theta} + \frac{1}{r^2}\frac{\partial\Phi}{\partial\theta} + \frac{\partial^2\Psi}{\partial r^2}, \\ m_{rz} &= \frac{\partial\Psi}{\partial r}, \;\; m_{\theta z} = \frac{1}{r}\frac{\partial\Psi}{\partial\theta}. \end{aligned} \tag{3}$$

The stresses/couple stresses and displacements/micro-rotations are related via the following expressions [3]:

$$\begin{aligned} \frac{\sigma_{rr}}{2G} &= \left(\frac{\partial u}{\partial r} + \frac{\nu}{1-2\nu}\left(\frac{\partial u}{\partial r} + \frac{1}{r}\frac{\partial v}{\partial\theta} + \frac{u}{r}\right)\right), \\ \frac{\sigma_{\theta\theta}}{2G} &= \left(\frac{1}{r}\frac{\partial v}{\partial\theta} + \frac{u}{r} + \frac{\nu}{1-2\nu}\left(\frac{\partial u}{\partial r} + \frac{1}{r}\frac{\partial v}{\partial\theta} + \frac{u}{r}\right)\right), \\ \frac{\sigma_{r\theta}}{G} &= \left(\frac{\partial v}{\partial r} + \frac{1}{r}\frac{\partial u}{\partial\theta} - \frac{v}{r}\right) + \frac{N^2}{1-N^2}\left(\frac{\partial v}{\partial r} - \frac{1}{r}\frac{\partial u}{\partial\theta} + \frac{v}{r} - 2\phi\right), \\ \frac{\sigma_{\theta r}}{G} &= \left(\frac{\partial v}{\partial r} + \frac{1}{r}\frac{\partial u}{\partial\theta} - \frac{v}{r}\right) - \frac{N^2}{1-N^2}\left(\frac{\partial v}{\partial r} - \frac{1}{r}\frac{\partial u}{\partial\theta} + \frac{v}{r} - 2\phi\right), \\ \frac{m_{rz}}{4\ell^2 G} &= \frac{\partial\phi}{\partial r}, \;\; \frac{m_{\theta z}}{4\ell^2 G} = \frac{1}{r}\frac{\partial\phi}{\partial\theta}. \end{aligned} \tag{4}$$

From the relation between displacements and stresses we can deduce

$$\begin{aligned} \frac{\partial u}{\partial r} &= \frac{1}{2G}((1-\nu)\sigma_{rr} - \nu\sigma_{\theta\theta}), \\ \frac{\partial v}{\partial r} &= \phi + \frac{1}{2G}\left(\left(\frac{1}{2} + \frac{1-N^2}{2N^2}\right)\sigma_{r\theta} + \left(\frac{1}{2} - \frac{1-N^2}{2N^2}\right)\sigma_{\theta r}\right), \end{aligned} \tag{5}$$

while the microrotation is expressed as

$$\phi = \frac{1}{4\ell^2 G}\Psi. \tag{6}$$

3 The inclusion problem

The inclusion problem is formulated as follows. We consider an inclusion of one micropolar material with constants G_1, ν_1, ℓ_1, N_1 into an infinite micropolar matrix described by constants G_2, ν_2, ℓ_2, N_2. The origin of the coordinate system is placed at the center of the inclusion and the radius of the inclusion is denoted as a. (Fig. 1). In what follows we will use indices $^{(i)}$ to denote all quantities related to the inclusion, while $^{(e)}$ will stand for the quantities related to the matrix.
The boundary conditions at $r \to \infty$ are given as

$$\begin{aligned} \sigma_{rr}^{(e)} &= \frac{\sigma_0}{2}(1+\cos 2\theta), \\ \sigma_{r\theta}^{(e)} &= -\frac{\sigma_0}{2}\sin 2\theta, \\ m_{rz}^{(e)} &= 0, \end{aligned} \tag{7}$$

while on the boundary of the inclusion $r = a$ we impose:

$$\begin{aligned} &(1)\ \ \lambda_r \sigma_{rr}^{(e)} = u^{(e)} - u^{(i)}, \\ &(2)\ \ \lambda_\theta \sigma_{r\theta}^{(e)} = v^{(e)} - v^{(i)}, \\ &(3)\ \ \lambda_\phi m_{rz}^{(e)} = \phi^{(e)} - \phi^{(i)}, \\ &(4)\ \ \sigma_{rr}^{(e)} = \sigma_{rr}^{(i)}, \\ &(5)\ \ \sigma_{r\theta}^{(e)} = \sigma_{r\theta}^{(i)}, \\ &(6)\ \ m_{rz}^{(e)} = m_{rz}^{(i)}, \end{aligned} \tag{8}$$

where constants $\lambda_r, \lambda_\theta, \lambda_\phi$ are the interface parameters. Eq.(8.1), (8.2), (8.4), (8.5) for plane elasticity were derived in [20] by representing the interface as a layer of third material (interphase) with "small" thickness and using asymptotic expansions of the displacements and radial stresses in this layer. The same procedure was repeated in this work for micropolar materials, and from the highest order derivatives in the equilibrium equations and the relations between microrotations and couple-stresses, we have concluded that the interface conditions for microrotations $\phi^{(i)}$, $\phi^{(e)}$ and couple-stresses $m_{rz}^{(i)}$, $m_{rz}^{(e)}$ have the form of (8.3) and (8.6).

Analogously with the classical elasticity [22], two important limiting cases are included into eqs.(8): when $\lambda_r = 0, \lambda_\theta = 0, \lambda_\phi = 0$ we recover the perfect interface conditions, i.e. the displacements and microrotations stay continuous; the case $\lambda_r \to \infty, \lambda_\theta \to \infty, \lambda_\phi \to \infty$ corresponds to complete debonding.

Next, we seek the stress functions $\Phi^{(e)}$, $\Psi^{(e)}$, $\Phi^{(i)}$, $\Psi^{(i)}$ satisfying eqns.(1),(2) in the form of the Fourier series expansion. Analogously to the solution of the circular hole problem, given in [3] and to the solution of the inclusion problem (for a perfect interface, in couple-stress elasticity), given in [15], it can be shown that the stress

functions have the following form:

$$\begin{aligned}
\Phi^{(e)} &= \frac{\sigma_0}{4} r^2 (1 - \cos 2\theta) + A_1 \ln r + \left(\frac{A_2}{r^2} + A_3 \right) \cos 2\theta, \\
\Psi^{(e)} &= \left(\frac{A_4}{r^2} + A_5 K_2 \left(r/c_2 \right) \right) \sin 2\theta, \\
\Phi^{(i)} &= B_1 r^2 + (B_2 r^2 + B_3 r^4) \cos 2\theta, \\
\Psi^{(i)} &= \left(B_4 r^2 + B_5 I_2 \left(r/c_1 \right) \right) \sin 2\theta,
\end{aligned} \tag{9}$$

where $I_2\left(r/c_1\right)$, $K_2\left(r/c_2\right)$ are modified Bessel functions of the first and second kind respectively. The compatibility conditions (2) are satisfied if

$$A_4 = 8(1-\nu_2) l_2^2 A_3, \quad B_4 = 24(1-\nu_1) l_1^2 B_3 \tag{10}$$

Next, the solution of the problem consists in the following steps:
a) using the stress functions (9) all stresses and couple-stresses are derived according to eq.(4),
b) then displacements and microrotations are obtained by integrating eqs.(5),
c) all expressions for stresses, couple-stresses, displacements and microrotations are substituted into the boundary conditions (8) and in each equation the coefficients of $\{1, \cos 2\theta, \sin 2\theta\}$ are collected. This results in 8 equations for unknown $\boldsymbol{X} = \{A_1, A_2, A_3, A_5, B_1, B_2, B_3, B_5\}$, written schematically as

$$\boldsymbol{M}\boldsymbol{X} = \boldsymbol{Y}. \tag{11}$$

d) after system (11) is solved, all stresses, couple-stresses, displacements and microrotations are obtained from eq.(4), (5).
The expressions for all stresses/couple stresses, displacements/microrotations, and the entries of matrix $\boldsymbol{M}$ and vector $\boldsymbol{Y}$ are given in Appendix A. The full derivation of the solution, as well as the final results, are given in [24], in the form of Mathematica files, which can be used to obtain numerical values of all parameters of the problem for any fixed material properties.

4 Numerical results

4.1 Perfect interface

The solution for the case of the perfect interface corresponds to $\lambda_r = \lambda_\theta = \lambda_\phi = 0$ or both - desplacements/microrotation and tractions/couple traction - being continuous across the inclusion interface, i.e.

$$\begin{aligned}
&\sigma_{rr}^{(e)} = \sigma_{rr}^{(i)}, \;\; \sigma_{r\theta}^{(e)} = \sigma_{r\theta}^{(i)}, \;\; m_{rz}^{(e)} = m_{rz}^{(i)}, \\
&u^{(e)} = u^{(i)}, \;\; v^{(e)} = v^{(i)}, \;\; \phi^{(e)} = \phi^{(i)}.
\end{aligned} \tag{12}$$

First we examine the dependence of the solution on the ratio $g = G_1/G_2$. In Fig.2, 3, the stress concentration factors, defined as

$$\mathrm{SCF} = \max\{\sigma_{\theta\theta}^{(i)}(\pi/2)/\sigma_0, \sigma_{\theta\theta}^{(e)}(\pi/2)/\sigma_0\} \tag{13}$$

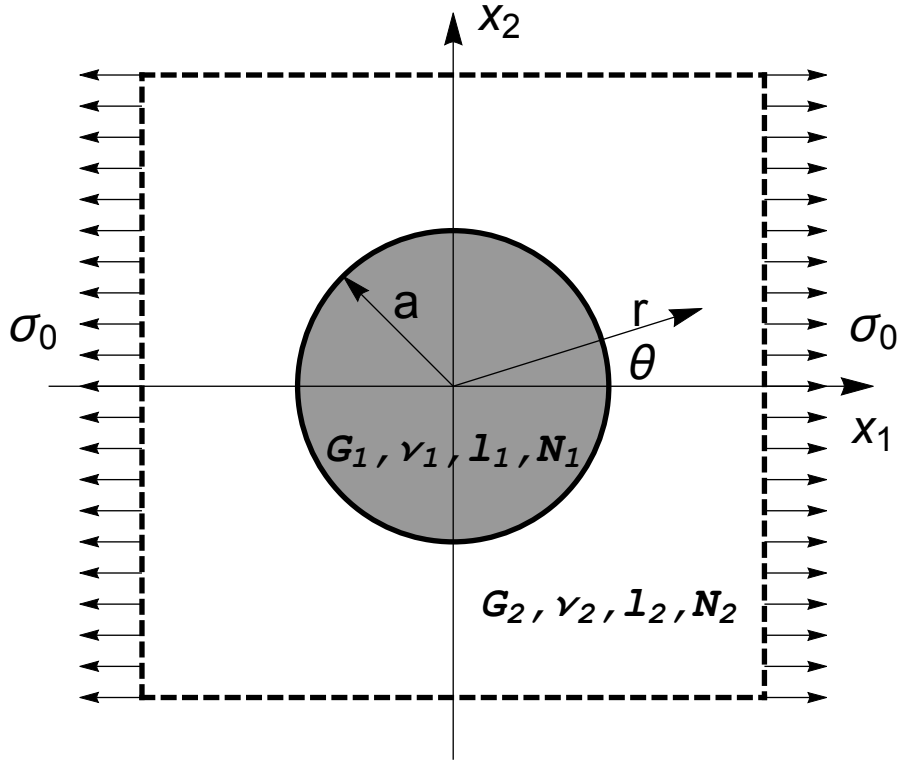

Figure 1: Circular inclusion in an infinite plate under uni-axial tension.

are shown for the fixed material parameters of the inclusion, i.e. $\ell_1/a = 0.75$, $N_1 = 0.5, \nu_1 = 0.25$ and various values of ℓ_2/a and N_2, while $\nu_2 = 1/3$. Note, that the maximum stress occurs in the inclusion for $g > g_\star$ and in the matrix for $g < g_\star$. The value of $g_\star$ is defined from the condition:

$$\sigma^{(e)}_{\theta\theta}(\pi/2) = \sigma^{(i)}_{\theta\theta}(\pi/2). \tag{14}$$

We have observed, that analogously to the classical elasticity, the value of $g_\star$ depends significantly on the values of ν_1 and ν_2. And $g_\star = 1$ for $\nu_1 = \nu_2$ independently of the values of all other material parameters.
As it can be seen from figure 2 for $g < g_\star$, the stress concentration factors for the same value of g reduce as ℓ_2/a and N_2 increase. Dependence of SCF on g for fixed values of ℓ_2/a and N_2 is analogous to the one in classical elasticity, where the higher stress concentrations are observed for softer inclusions. The case $g = 0$ corresponds to the problem of a infinite plate with a circular hole with the well-known solution given in [3].

For $g > g^\star$ the stress concentration factors given by $\sigma^{(i)}(\pi/2)/\sigma_0$ are plotted in fig. 3, also as functions of g. In the cases, when the matrix is softer than the inclusion, the stress concentration factors for the same value of g are greater for greater values of ℓ_2/a and N_2. As values of N_2 and ℓ_2/a increase, the solutions slower tend to their limiting values as $g \to \infty$. The limiting case of $g \to \infty$ corresponds to the solution of a problem of a rigid inclusion and it is given by dashed lines in fig. 3.

Next, we examine the dependence of the stress concentration factors on the values of the characteristic lengths. In fig.4, 5 the stress concentration factors, given by

$\sigma^{(e)}_{\theta\theta}(\pi/2)/\sigma_0$ for $g = 0.5$ and by $\sigma^{(i)}_{\theta\theta}(\pi/2)/\sigma_0$ for $g = 2$ are plotted as functions of the inclusion material length ℓ_1/a for various values of the matrix material parameters N_2, ℓ_2/a. The rest of the constants were fixed to: $\nu_1 = 0.25$, $\nu_2 = 1/3$, $N_1 = 0.5$. In the case of a "softer" inclusion in fig.4, the value of the SCF decreases as ℓ_2/a and N_2 increase, while for a "stiffer" inclusion in fig.4 the value of SCF increases as ℓ_2/a and N_2 increase.

The dependence of the SCFs on the value of the coupling number N_1 is shown in fig.6, 7 for various values of ℓ_2/a and N_2. Analogously to the previous plots, the biggest deviations from the classical solutions are observed as ℓ_2/a and N_2 increase.
Next, we analyse two limiting cases:
a) micropolar inclusion embedded in a matrix, described by classical elasticity,
b) classical inclusion embedded in a micropolar matrix.

a) Micropolar inclusion embedded in a matrix, described by classical elasticity. In this case we keep $\nu_1 = 0.25$, $\nu_2 = \frac{1}{3}$. The limiting values were taken for $N_2 = 0.001$, $\ell_2/a = 0.001$. The stress concentration factors $\sigma^{(e)}_{\theta\theta}(\pi/2)$ for $g = 0.5$ and $\sigma^{(i)}_{\theta\theta}(\pi/2)$ for $g = 2$ are shown in Fig. 8, 9 as functions of ℓ_1/a and N_1. In all four cases the values of the SCFs do not depend on ℓ_1/a and N_1 and coincide with the classical solution, given by $\sigma^{(e)}_{\theta\theta}(\pi/2) = 1.57576$ for $g = 0.5$ and $\sigma^{(i)}_{\theta\theta}(\pi/2) = 1.14872$ for $g = 2$. This conclusion is consistent with the results established in [15] for the case of the couple-stress elasticity.

a) Classical inclusion embedded in a micropolar matrix. In this case we keep $\nu_1 = 0.25$, $\nu_2 = \frac{1}{3}$. The limiting values were taken for $N_1 = 0.001$, $\ell_1/a = 0.001$. The stress concentration factors $\sigma^{(e)}_{\theta\theta}(\pi/2)$ for $g = 0.5$ and $\sigma^{(i)}_{\theta\theta}(\pi/2)$ for $g = 2$ are shown in Fig.10, 11 as functions of ℓ_1/a and N_1. In this case the stress intensity factors exhibit strong dependence on the parameters ℓ_2/a and N_2, which can be seen in figures 10, 11, and analogously to the previous plots, increasing micropolar parameters of the matrix leads to decreasing the value of SCF in the case of a softer inclusion and increasing the value of SCF in the case of a stiffer inclusion.

4.2 Imperfect interface

In the case of an imperfect interface, the distribution of stresses around the inclusion depends significantly on the bonding between the matrix and the inclusion, described by parameters λ_n, λ_s, λ_ϕ. It is noted, that analogously to the classical elasticity, for certain combinations of the interface parameters and the material parameters of the matrix and the inclusion, the interface model (8) yields negative displacement jumps. In such case, since the model is based on the asymptotic expansion of stresses and displacements in a thin "interphase" layer between the inclusion and the matrix, negative displacement jumps are still physically admissible, provided that they are sufficiently small. This issue is discussed in details in [22] and, since the similar reasoning is applicable in the case of micropolar elasticity, the detailed study is not provided in the present work.

For further analysis we introduce the non-dimensional parameters h_r, h_θ, h_ϕ :

$$\lambda_r = \frac{h_r}{G_2}, \lambda_\theta = \frac{h_\theta}{G_2}, \lambda_\phi = \frac{h_\phi}{G_2}. \tag{15}$$

In fig.12 we demonstrate the dependence of $\sigma^{(i)}_{\theta\theta}$, $\sigma^{(e)}_{\theta\theta}$ at point $\theta = \pi/2$ on g for

$h_\phi = 0.1$ and various values of interface parameters h_r and h_θ. As it can be seen from fig.12(a) in the case of perfect bonding in r direction, maximum hoop stress is observed in the matrix for all values of g, while in the case of perfect bonding in θ direction only (fig.12(b)), maximum hoop stress is observed in the matrix for $g < g^\star = 1.0355$ and in the inclusion for $g > g^\star = 1.0355$. The same tendency is demonstrated in fig.12 (c) for $h_r = h_\theta = 0.25$, however in this case $g^\star = 2.4751$. In fig.12 (d) the values of $\sigma_{\theta\theta}$ are shown for $h_r = h_\theta = 1$, where the stress concentration is always observed in the matrix.

The same tendency is illustrated in fig.13 for $g = 0.5$ and fig.14 for $g = 2$. Values of $\sigma^{(e)}_{\theta\theta}(\pi/2)$, $\sigma^{(i)}_{\theta\theta}(\pi/2)$ are plotted as functions of $h = h_r = h_\theta$ and $p = h_\phi$. In the case of $g = 0.5$, for all values of parameters of h and p the values of $\sigma^{(e)}_{\theta\theta}(\pi/2)$ are greater than the value of $\sigma^{(i)}_{\theta\theta}(\pi/2)$, while in the case of $g = 2$ for small values of h and any p - the higher stress is observed in the inclusion, but for greater values of h the values of $\sigma^{(e)}_{\theta\theta}(\pi/2)$ become greater than the values of $\sigma^{(i)}_{\theta\theta}(\pi/2)$.

As can be seen in fig.13, 14 for values of p in the range from 0 to 10, dependence of the solutions on p is much smaller than the dependence on h. For the material parameters used in this example, and for $h = 0$, $g = 2$ the difference in $SCF = \max \sigma^{(e)}_{\theta\theta}(\pi/2), \sigma^{(i)}_{\theta\theta}(\pi/2)$ between $p = 0$ and $p = \infty$ is about $+2\%$. For $h = \infty$, $g = 2$ the difference in SCF between $p = 0$ and $p = \infty$ is about -6%.

Another property of the imperfect interface is that for some fixed material parameters the interface parameters can be chosen in such way, that no stress concentration occurs. For example, for the material data, used in Fig.14 in the case $g = 2.0$ and $p = 1$ choosing $h = 0.2149$ leads to $\sigma^{(i)}_{\theta\theta}(\pi/2)/\sigma_0 = \sigma^{(e)}_{\theta\theta}(\pi/2)/\sigma_0 = 0.99755$. However, this cannot be achieved in the case $g = 0.5$, as it can be seen from Fig.14, for all combinations of p and h, the minimum value of $\sigma^{(e)}_{\theta\theta}(\pi/2)/\sigma_0 = 1.272$ while the maximum value $\sigma^{(e)}_{\theta\theta}(\pi/2)/\sigma_0 = 0.792$.

Next, in Fig.15,16, we demonstrate the influence of parameter h on the distribution of σ_{rr}, $\sigma_{r\theta}$ and couple stress m_{rz} along the inclusion interface. In all cases increasing h leads to decreasing σ_{rr} and increasing magnitude of $\sigma_{r\theta}$. However, some values of h for $g = 2.0$ lead to negative couple stress m_{rz}.

And finally, in Fig.17 we plot the maximum values $U^\star$ of the normalized interface energy density $U(\theta)$ as a function of interface parameter $h = \lambda_r = \lambda_\theta$ for various values of parameter $p = \lambda_\phi$. Function $U(\theta)$ is defined analogously to [22], but with taking into account the contribution from the couple-stresses, i.e.

$$U(\theta) = \lambda_r \sigma^2_{rr} + \lambda_\theta \sigma^2_{r\theta} + \lambda_\phi m^2_{rz}. \tag{16}$$

Function $U(\theta)$ reaches its maximum at $\theta = 0$, i.e. $U^\star = U(0)$, where the interface failure is most likely to occur. As it can be seen from Fig.13, 14 the influence of parameter p on maximum value of $U(\theta)$ is less significant in comparison with the influence of parameter h. Plots, analogous to the ones in Fig.17 can be used in material design to choose interface parameters in order not to exceed the prescribed critical value of $U^\star$, corresponding to the failure of the interface.

5 Conclusions

In the present work, we developed an analytical solution for the problem of an inhomogeneity in plane micropolar elasticity. We studied the dependence of the stress

concentration on the material parameters, as well as the parameters characterizing bonding between the inhomogeneity and the matrix.

Some of the main results are qualitatively described below:

- In the case of a perfect interface, for fixed material parameters of the inclusion, increasing micropolar parameters of the matrix (ℓ_2/a, N_2) leads to significant decrease of the stress concentration for softer inclusions and increase of the stress concentration for stiffer inclusions.
- In the case of a perfect interface, if the matrix's microstructural effects are absent, i.e. $l_2/a = N_2 = 0$, the stress concentration does not depend on the micropolar parameters of the inclusion and equals to the value, described by the classical theory of elasticity.
- Results also show that in some cases of the imperfect interface, for fixed material parameters, the interface parameters can be chosen in such way, that no stress concentration occurs.

The solution can be further used to study interface failure in presence of microstructural effects or for verification of numerical methods.

6 Acknowledgements

The work presented in this paper was partially supported by Fondecyt grant number 11130259 entitled "Boundary element modeling of crack propagation in micropolar materials".

References

[1] Cosserat, E., Cosserat, F. Sur la theorie de l'elasticite, Ann. de l'Ecole Normale de Toulouse, 10, 1, 1 (1896).

[2] Eringen, A.C. Linear theory of micropolar elasticity, J. Math. Mech. 15**,** 909 - 923 (1966).

[3] Eringen A.C. Microcontinuum Field Theories. 1999

[4] Nowacki, W. Theory of asymmetric elasticity, Polish Scientific Publishers, Warsaw, 1986.

[5] Bigoni, D., Drugan, W.J., Analytical Derivation of Cosserat Moduli via Homogenization of Heterogeneous Elastic Materials, J. Appl. Mech. 74(4), 741-753, doi:10.1115/1.2711225

[6] Forest, S., Pradel, F., Sab, K., Asymptotic analysis of heterogeneous Cosserat media, International Journal of Solids and Structures, 38 (26-27), pp.4585 - 4608, 2001, doi:10.1016/S0020-7683(00)00295-X

[7] Lakes, R. Experimental micro mechanics methods for conventional and negative Poisson's ratio cellular solids as Cosserat continua, J. Engng. Materials and Tech., 113, 148-155 (1991).

[8] Lakes, R. Experimental methods for study of Cosserat elastic solids and other generalized elastic continua, in Continuum Models for Materials with Microstructure (edited by H.B. Muhlhaus), pp. 1-13, John Wiley and Sons, 1995

[9] Nakamura S, Lakes RS. Finite element analysis of stress concentration around a blunt crack in a Cosserat elastic solid. Comp Meth Appl Mech Eng 1988; 66: 257266

[10] Lei Li, Shuisheng Xie, Finite element method for linear micropolar elasticity and numerical study of some scale effects phenomena in MEMS, International Journal of Mechanical Sciences, 46(11), 2004, 15711587, DOI:10.1016/j.ijmecsci.2004.10.004

[11] Diegele, E. Elser, R. Tsakmakis, C., Linear micropolar elastic crack-tip fields under mixed mode loading conditions, International Journal of Fracture, 10/2004; 129(4):309-339. DOI: 10.1023/B:FRAC.0000049492.13523.5a

[12] K.Z. Liang, F.Y. Huang, Boundary element method for micropolar elasticity, International Journal of Engineering Science, 34 (1996), pp. 509521

[13] Atroshchenko E., Bordas S., Fundamental solutions and dual boundary element methods for fracture in plane Cosserat elasticity, Proc. R. Soc. A 471 (2179), 20150216

[14] M.A. Kulesh, V.P. Matveenko, I.N. Shardakov, Parametric analysis of analytical solutions to one- and two-dimensional problems in couple-stress theory of elasticity, ZAMM, 83(4), pages 238248, 2003, DOI: 10.1002/zamm.200310031

[15] Weitsmann, Y. Couple-stress effects on stress concentration around a cylindrical inclusion in a field of uniaxial tension, J. Appl. Mech, 6, 424-427 (1965).

[16] R. J. Hartranft and G. C. Sih, The Effect of Couple-Stresses on the Stress Concentration of a Circular Inclusion, J. Appl. Mech 32(2), 429-431, 1965

[17] J.D. Achenbach and H. Zhu, Effect of interfacial zone on mechanical behavior and failure of fiber-reinforced composites, Journal of the Mechanics and Physics of Solids, 37(3), 381 - 393, 1989

[18] Zvi Hashin, Thermoelastic properties of particulate composites with imperfect interface, Journal of the Mechanics and Physics of Solids, 39(6), 745 - 762, 1991

[19] Zvi Hashin, Extremum principles for elastic heterogenous media with imperfect interfaces and their application to bounding of effective moduli, Journal of the Mechanics and Physics of Solids, 40(4), 767 - 781, 1992

[20] D Bigoni, SK Serkov, M Valentini, AB Movchan, Asymptotic models of dilute composites with imperfectly bonded inclusions, International Journal of Solids and Structures 35 (24), 3239-3258

[21] L.J. Sudak, C.Q. Ru, P. Schiavone, A. Mioduchowski, A circular inclusion with inhomogeneously imperfect interface in plane elasticity J. Elasticity, 55 (1999), pp. 1941

[22] H. Shen, P. Schiavone, C.Q. Ru, A. Mioduchowski, Stress analysis of an elliptic inclusion with imperfect interface in plane elasticity J. Elasticity, 62 (2001), pp. 2546

[23] Xu Wang, , Junqian Zhang, Xingming Guo, Two circular inclusions with inhomogeneously imperfect interfaces in plane elasticity, International Journal of Solids and Structures, Volume 42, Issues 910, 2005, doi:10.1016/j.ijsolstr.2004.10.002

[24] Analytical solution for the problem of a micropolar inclusion in an infinite plate subjected to uni-axial remote tension, https://sourceforge.net/projects/micropolarinclusion/

A Apendix

The equations for stresses and couple stresses in the matrix are identical to those derived in [3] for the problem of a plate with a hole and are given as follows.

$$
\begin{aligned}
\sigma_{rr}^{(e)}(r,\theta) &= \frac{\sigma_0}{2}(1+\cos 2\theta) + \frac{A_1}{r^2} - \left(\frac{6A_2}{r^4} + \frac{4A_3}{r^2} - \frac{6A_4}{r^4}\right)\cos 2\theta \\
&\quad + \frac{2A_5}{c_2 r}\left[\frac{3c_2}{r}K_0(r/c_2) + \left(1+\frac{6c_2^2}{r^2}\right)K_1(r/c_2)\right]\cos 2\theta, \\
\sigma_{\theta\theta}^{(e)}(r,\theta) &= \frac{\sigma_0}{2}(1-\cos 2\theta) - \frac{A_1}{r^2} + \left(\frac{6A_2}{r^4} - \frac{6A_4}{r^4}\right)\cos 2\theta \\
&\quad - \frac{2A_5}{c_2 r}\left[\frac{3c_2}{r}K_0(r/c_2) + \left(1+\frac{6c_2^2}{r^2}\right)K_1(r/c_2)\right]\cos 2\theta, \\
\sigma_{r\theta}^{(e)}(r,\theta) &= -\left(\frac{\sigma_0}{2} + \frac{6A_2}{r^4} + \frac{2A_3}{r^2} - \frac{6A_4}{r^4}\right)\sin 2\theta \\
&\quad + \frac{A_5}{c_2 r}\left[\frac{6c_2}{r}K_0(r/c_2) + \left(1+\frac{12c_2^2}{r^2}\right)K_1(r/c_2))\right]\sin 2\theta, \\
\sigma_{\theta r}^{(e)}(r,\theta) &= -\left(\frac{\sigma_0}{2} + \frac{6A_2}{r^4} + \frac{2A_3}{r^2} - \frac{6A_4}{r^4}\right)\sin 2\theta \\
&\quad + \frac{A_5}{c_2^2}\left[\left(1+\frac{6c_2^2}{r^2}\right)K_0(r/c_2) + \left(\frac{3c_2}{r}+\frac{12c_2^3}{r^3}\right)K_1(r/c_2)\right]\sin 2\theta, \\
m_{rz}^{(e)}(r,\theta) &= \left(-\frac{2A_4}{r^3} - \frac{A_5}{c_2}\left[\frac{2c_2}{r}K_0(r/c_2) + \left(1+\frac{4c_2^2}{r^2}\right)K_1(r/c_2)\right]\right)\sin 2\theta, \\
m_{\theta z}^{(e)}(r,\theta) &= \left(\frac{2A_4}{r^3} + \frac{2A_5}{r}\left[K_0(r/c_2) + \frac{2c_2}{r}K_1(r/c_2)\right]\right)\cos 2\theta.
\end{aligned}
\tag{17}
$$

The equations for stresses and couple stresses in the inclusion are similar to those derived in [15] for the problem of a circular inclusion in couple-stress elasticity and are

given as follows.

$$
\begin{aligned}
\sigma_{rr}^{(i)}(r,\theta) &= 2B_1 - 2(B_2+B_4)\cos 2\theta \\
&\quad + \frac{2B_5}{c_1 r}\left[\frac{3c_1}{r}I_0(r/c_1) - \left(1+\frac{6c_1^2}{r^2}\right)I_1(r/c_1)\right]\cos 2\theta, \\
\sigma_{\theta\theta}^{(i)}(r,\theta) &= 2B_1 + 2(B_2+B_4+6B_3r^2)\cos 2\theta \\
&\quad + \frac{2B_5}{c_1 r}\left[-\frac{3c_1}{r}I_0(r/c_1) + \left(1+\frac{6c_1^2}{r^2}\right)I_1(r/c_1)\right]\cos 2\theta, \\
\sigma_{r\theta}^{(i)}(r,\theta) &= 2(B_2+B_4+3B_3r^2)\sin 2\theta \\
&\quad + \frac{B_5}{c_1 r}\left[\frac{6c_1}{r}I_0(r/c_1) - \left(1+\frac{12c_1^2}{r^2}\right)I_1(r/c_1)\right]\sin 2\theta, \\
\sigma_{\theta r}^{(i)}(r,\theta) &= 2(B_2+B_4+3B_3r^2)\sin 2\theta \\
&\quad + \frac{B_5}{c_1^2}\left[\left(1+\frac{6c_1^2}{r^2}\right)I_0(r/c_1) - \left(\frac{3c_1}{r}+\frac{12c_1^3}{r^3}\right)I_1(r/c_1)\right]\sin 2\theta, \\
m_{rz}^{(i)}(r,\theta) &= \left(2B_4 r + \frac{B_5}{c_1}\left[-\frac{2c_1}{r}I_0(r/c_1) + \left(1+\frac{4c_1^2}{r^2}\right)I_1(r/c_1)\right]\right)\sin 2\theta, \\
m_{\theta z}^{(i)}(r,\theta) &= \left(2B_4 r + \frac{2B_5}{r}\left[I_0(r/c_1) - \frac{2c_1}{r}I_1(r/c_1)\right]\right)\cos 2\theta.
\end{aligned}
\tag{18}
$$

Displacements and microrotations are given as:

$$
\begin{aligned}
2G_2 u^{(e)} &= \frac{r\sigma_0}{2}(1-2\nu_2+\cos 2\theta) - \frac{A_1}{r} \\
&\quad + \left(\frac{2(A_2-A_4)}{r^3} + \frac{4A_3(1-\nu_2)}{r} - \frac{2A_5K_2(r/c_2)}{r}\right)\cos 2\theta, \\
2G_2 v^{(e)} &= -\frac{r\sigma_0}{2}\sin 2\theta + \left(\frac{2(A_2-A_4)}{r^3} - \frac{2A_3(1-2\nu_2)}{r}\right)\sin 2\theta, \\
&\quad - \frac{A_5}{c_2}\left[\frac{2c_2}{r}K_0(r/c_2) + \left(1+\frac{4c_2^2}{r^2}\right)K_1(r/c_2)\right]\sin 2\theta, \\
4G_2 l_2^2 \phi^{(e)} &= \left(\frac{A_4}{r^2} + A_5K_2(r/c_2)\right)\sin 2\theta,
\end{aligned}
\tag{19}
$$

$$
\begin{aligned}
2G_1 u^{(i)} &= 2r(1-2\nu_1)B_1 \\
&\quad - \left(2r(B_2+B_4) + 4B_3\nu_1 r^3 + \frac{2B_5}{r}I_2(r/c_1)\right)\cos 2\theta, \\
2G_1 v^{(i)} &= (2r(B_2+B_4) + 2B_3r^3(3-2\nu_1))\sin 2\theta \\
&\quad + \frac{B_5}{c_1}\left[-\frac{2c_1}{r}I_0(r/c_1) + \left(1+\frac{4c_1^2}{r^2}\right)I_1(r/c_1)\right]\sin 2\theta, \\
4G_1 l_1^2 \phi^{(i)} &= \big(B_4 r^2 + B_5 I_2(r/c_1)\big)\sin 2\theta,
\end{aligned}
\tag{20}
$$

The boundary conditions (8) yield the following system of linear algebraic equations for unknown coefficients $\boldsymbol{X} = \{A_1, A_2, A_3, A_5, B_1, B_2, B_3, B_5\}$:

$$
\boldsymbol{M}\boldsymbol{X} = \boldsymbol{Y}, \tag{21}
$$

where the coefficients of matrix $\boldsymbol{M}$ are given by

$$
\begin{aligned}
&M_{11}=0, M_{12}=\frac{1}{a^3G_2}+\frac{6\lambda_r}{a^4},\\
&M_{13}=\frac{2(1-\nu_2)}{aG_2}-\frac{8\ell_2^2(1-\nu_2)}{a^3G_2}+\lambda_r\left(\frac{4}{a^2}-\frac{48\ell_2^2(1-\nu_2)}{a^4}\right)\\
&M_{14}=-\frac{K_0(a/c_2)}{aG_2}-\frac{2c_2K_1(a/c_2)}{a^2G_2}-\lambda_r\left(\frac{6K_2(a/c_2)}{a^2}+\frac{2K_1(a/c_2)}{ac_2}\right)\\
&M_{15}=0, M_{16}=a/G_1, M_{17}=\frac{24a\ell_1^2(1-\nu_2)}{G_1}+\frac{2a^3\nu_1}{G_1}, M_{18}=\frac{I_2(a/c_1)}{aG_1},\\
&M_{21}=-\frac{1}{2aG_2}-\frac{\lambda_r}{a^2}, M_{22}=M_{23}=M_{24}=0, M_{25}=\frac{a\left(-1+2\nu_1\right)}{G_1},\\
&M_{26}=M_{27}=M_{28}=M_{31}=0, M_{32}=\frac{1}{a^3G_2}+\frac{6\lambda_\theta}{a^4},\\
&M_{33}=\frac{-1+2\nu_2}{aG_2}-\frac{8\ell_2^2\left(1-\nu_2\right)}{a^3G_2}+\lambda_\theta\left(\frac{2}{a^2}-\frac{48\ell_2^2\left(1-\nu_2\right)}{a^4}\right),\\
&M_{34}=-\frac{K_0(a/c_2)}{aG_2}-\frac{K_1(a/c_2)}{2c_2G_2}\left(1+\frac{4c_2^2}{a^2}\right)-\lambda_\theta\left(\frac{6K_2(a/c_2)}{a^2}+\frac{K_1(a/c_2)}{ac_2}\right),\\
&M_{35}=0, M_{36}=-\frac{a}{G_1}, M_{37}=\frac{a^3\left(2\nu_1-3.\right)}{G_1}-\frac{24a\ell_1^2\left(1-\nu_1\right)}{G_1},\\
&M_{38}=\frac{I_0(a/c_1)}{aG_1}-\frac{I_1(a/c_1)}{2c_1G_1}\left(1+\frac{4c_1^2}{a^2}\right),\\
&M_{41}=M_{42}=0, M_{43}=\frac{2(1-\nu_2)}{a^2G_2}+\frac{16\ell_2^2\left(1-\nu_2\right)\lambda_\phi}{a^3},\\
&M_{44}=\frac{K_2(a/c_2)}{4G_2\ell_2^2}+\frac{\lambda_\phi\left(K_1(a/c_2)+K_3(a/c_2)\right)}{2c_2},\\
&M_{45}=M_{46}=0, M_{47}=-\frac{6a^2(1-\nu_1)}{G_1}, M_{48}=-\frac{I_2(a/c_1)}{4G_1\ell_1^2},\\
&M_{51}=0, M_{52}=-\frac{6}{a^4}, M_{53}=-\frac{4}{a^2}+\frac{48\ell_2^2\left(1-\nu_2\right)}{a^4}, M_{54}=\frac{6K_2(a/c_2)}{a^2}+\frac{2K_1(a/c_2)}{ac_2},\\
&M_{55}=0, M_{56}=2, M_{57}=48\ell_1^2(1-\nu_1), M_{58}=\frac{2I_1(a/c_1)}{ac_1}-\frac{6I_2(a/c_1)}{a^2},\\
&M_{61}=\frac{1}{a^2}, M_{62}=M_{63}=M_{64}=0, M_{65}=-2, M_{66}=M_{67}=M_{68}=0,\\
&M_{71}=0, M_{72}=-\frac{6}{a^4}, M_{73}=-\frac{2}{a^2}+\frac{48\ell_2^2\left(1-\nu_2\right)}{a^4}, M_{74}=\frac{6K_2(a/c_2)}{a^2}+\frac{K_1(a/c_1)}{ac_2},\\
&M_{75}=0, M_{76}=-2, M_{77}=-6a^2-48\ell_1^2(1-\nu_1), M_{78}=\frac{I_1(a/c_1)}{ac_1}-\frac{6I_2(a/c_1)}{a^2},\\
&M_{81}=M_{82}=0, M_{83}=-\frac{16\ell_2^2(1-\nu_2)}{a^3}, M_{84}=-\frac{K_1(a/c_2)+K_3(a/c_2)}{2c_2},\\
&M_{85}=M_{86}=0, M_{87}=-48a\ell_1^2(1-\nu_1), M_{88}=-\frac{I_1(a/c_1)+I_3(a/c_1)}{2c_1}.
\end{aligned}
\tag{22}
$$

And vector $\boldsymbol{Y}$ is given by:

$$\begin{aligned} &Y_1 = -\frac{a\sigma_0}{4G_2} + \frac{\sigma_0\lambda_r}{2}, Y_2 = -\frac{a\sigma_0}{4G_2} + \frac{a\sigma_0\nu_2}{2G_2} + \frac{\sigma_0\lambda_r}{2}, Y_3 = \frac{a\sigma_0}{4G_2} - \frac{\sigma_0\lambda_\theta}{2}, \\ &Y_4 = 0, Y_5 = Y_6 = -\frac{\sigma_0}{2}, Y_7 = \frac{\sigma_0}{2}, Y_8 = 0. \end{aligned} \tag{23}$$

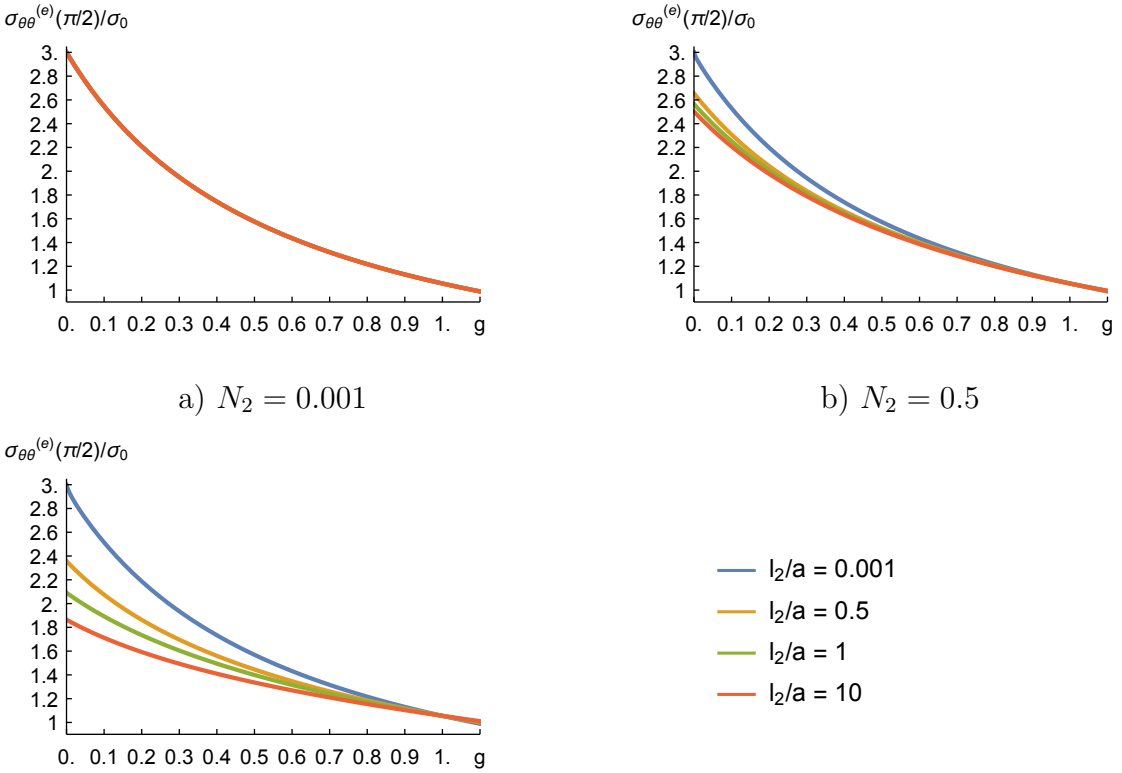

a) $N_2 = 0.001$

b) $N_2 = 0.5$

c) $N_2 = 1$

Figure 2: Stress concentration factor $\sigma_{\theta\theta}^{(e)}(\pi/2)/\sigma_0$ for $\ell_1/a = 0.75$, $\nu_1 = 0.25$, $N_1 = 0.5$, $\nu_2 = 1/3$ and various values of ℓ_2/a and N_2 as function of $g = G_1/G_2$.

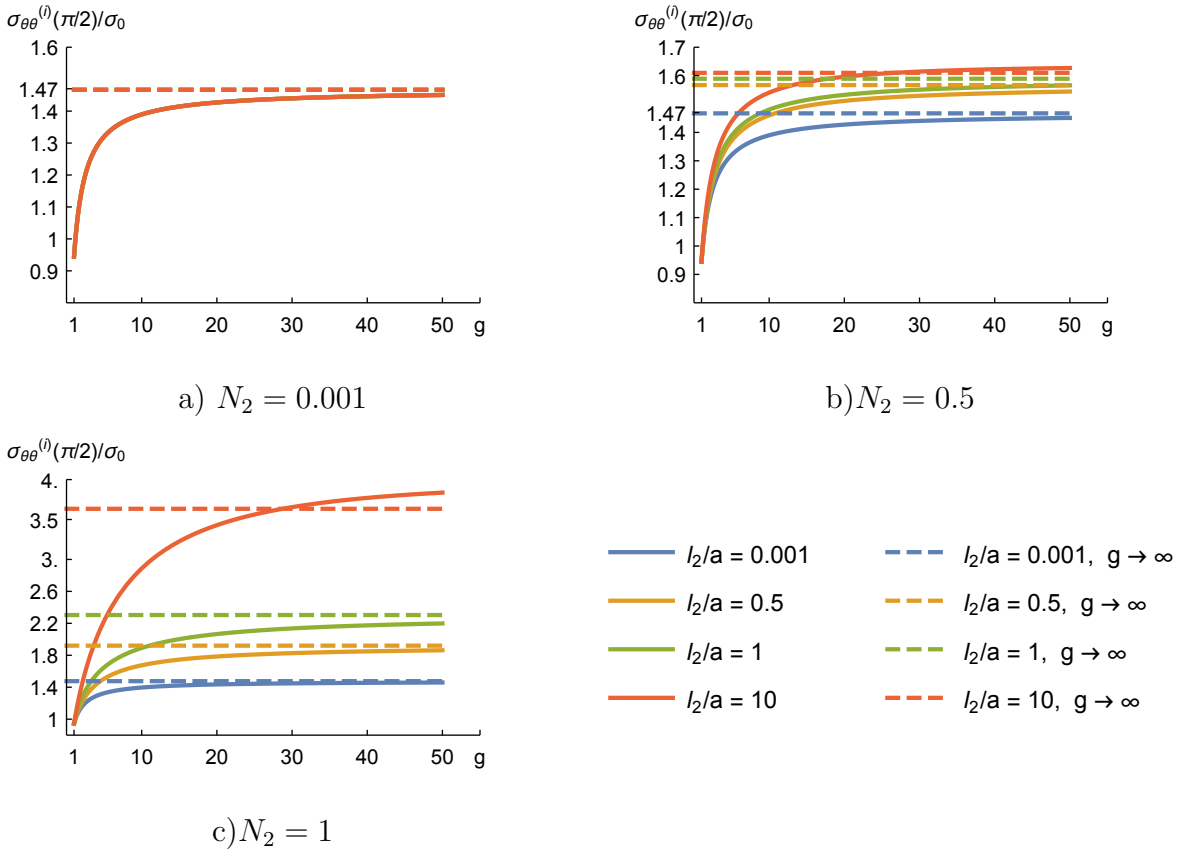

Figure 3: Stress concentration factor $\sigma_{\theta\theta}^{(i)}(\pi/2)/\sigma_0$ for $\ell_1/a = 0.75$, $\nu_1 = 0.25$, $N_1 = 0.5$, $\nu_2 = 1/3$ and various values of ℓ_2/a and N_2 as function of $g = G_1/G_2$.

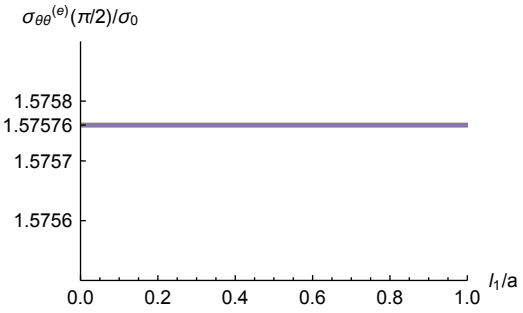

a)$N_2 = 0.001$

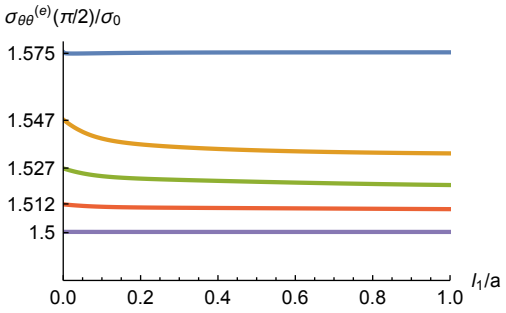

b)$N_2 = 0.5$

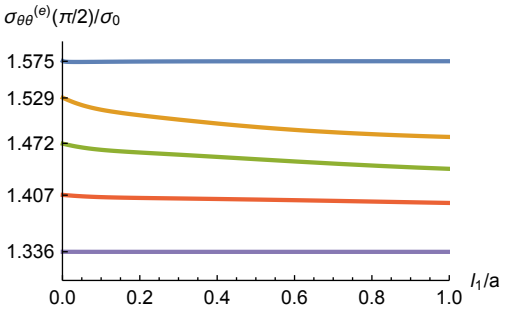

c)$N_2 = 1$

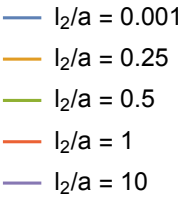

Figure 4: Stress concentration factor $\sigma_{\theta\theta}^{(e)}(\pi/2)$ for $g = 0.5$, $\nu_1 = 0.25$, $N_1 = 0.5$, $\nu_2 = 1/3$ and various values of ℓ_2/a and N_2 as function of ℓ_1/a.

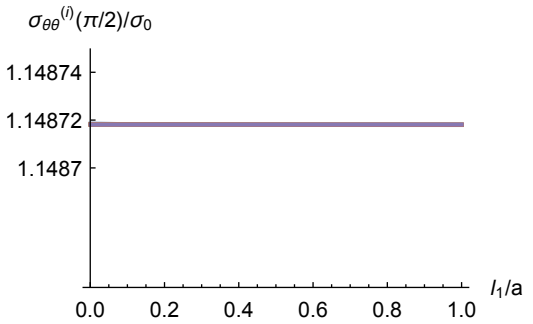

a)$N_2 = 0.001$

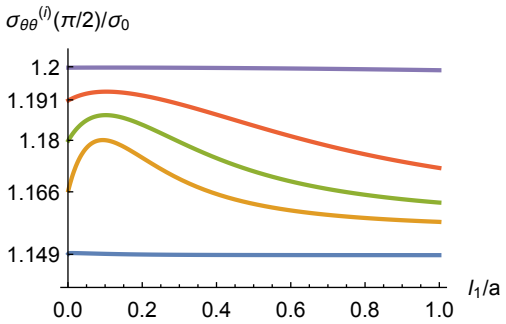

b)$N_2 = 0.5$

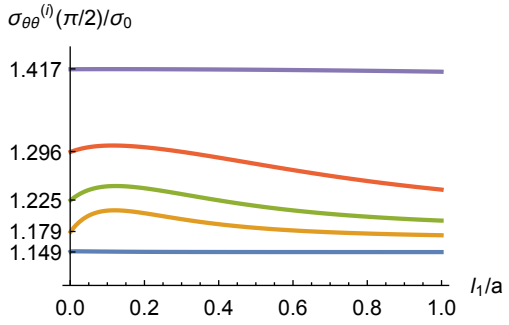

c)$N_2 = 1$

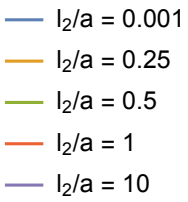

Figure 5: Stress concentration factor $\sigma_{\theta\theta}^{(i)}(\pi/2)$ for $g = 2$, $\nu_1 = 0.25$, $N_1 = 0.5$, $\nu_2 = 1/3$ and various values of ℓ_2/a and N_2 as function of ℓ_1/a.

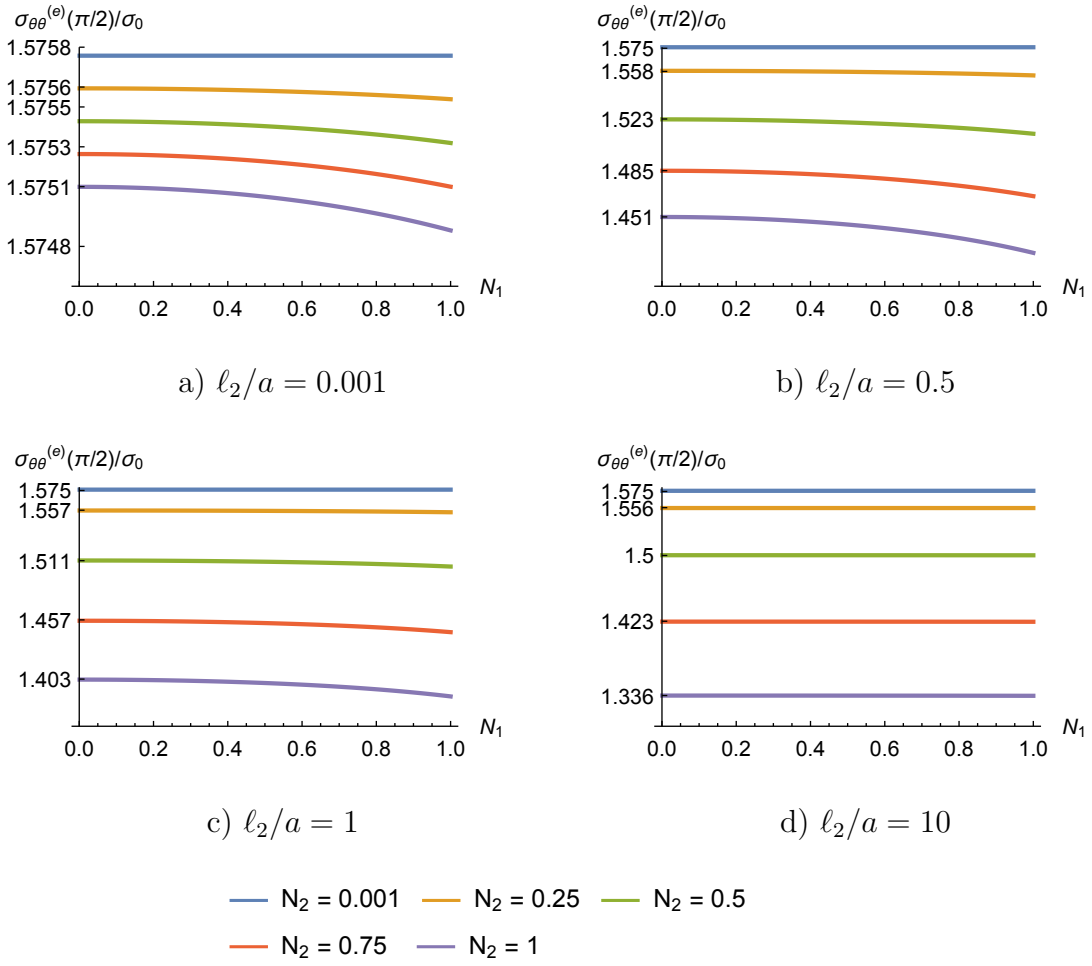

a) $\ell_2/a = 0.001$

b) $\ell_2/a = 0.5$

c) $\ell_2/a = 1$

d) $\ell_2/a = 10$

Figure 6: Stress concentration factor $\sigma_{\theta\theta}^{(e)}(\pi/2)$ for $g = 0.5$, $\nu_1 = 0.25$, $\ell_1 = 0.75$, $\nu_2 = 1/3$ and various values of ℓ_2/a and N_2 as function of N_1.

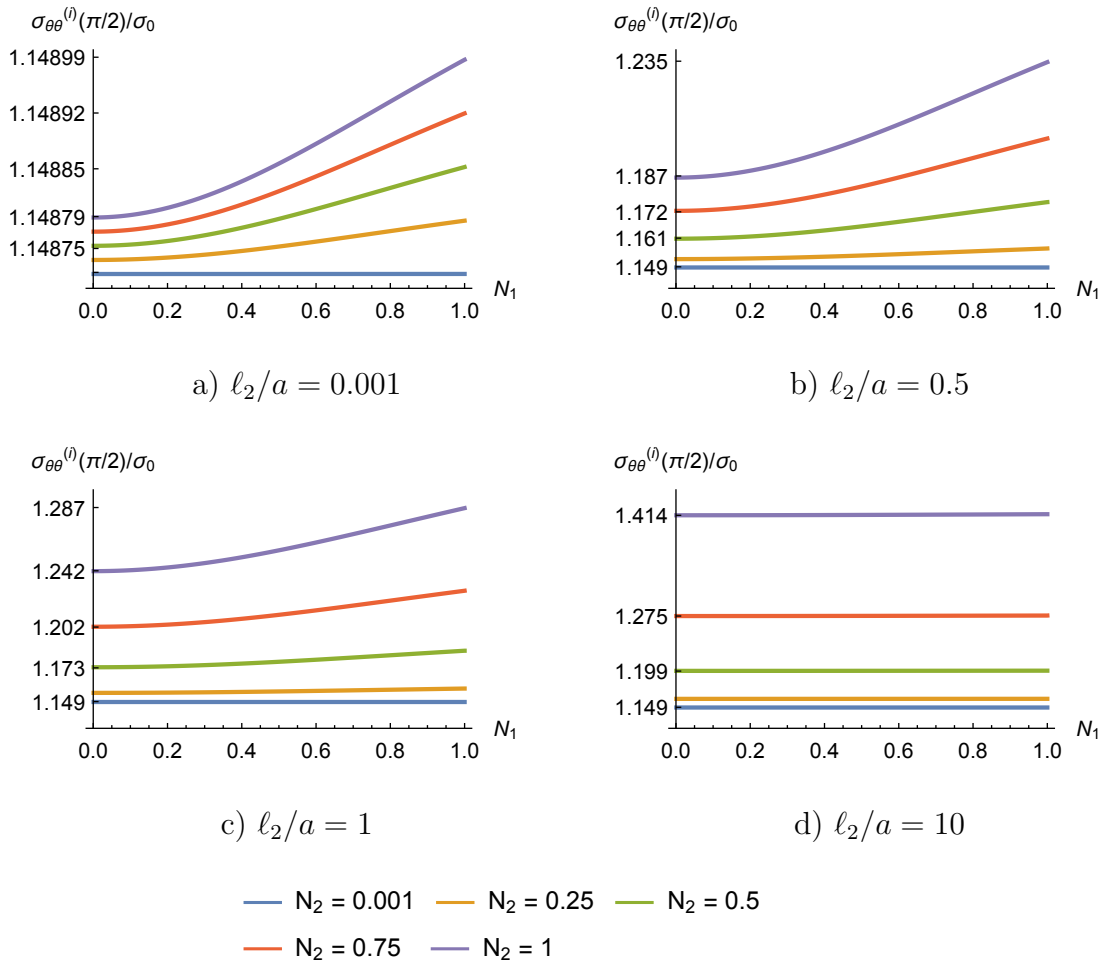

Figure 7: Stress concentration factor $\sigma_{\theta\theta}^{(i)}(\pi/2)$ for $g = 2$, $\nu_1 = 0.25$, $\ell_1/a = 0.75$, $\nu_2 = 1/3$ and various values of ℓ_2/a and N_2 as function of N_1.

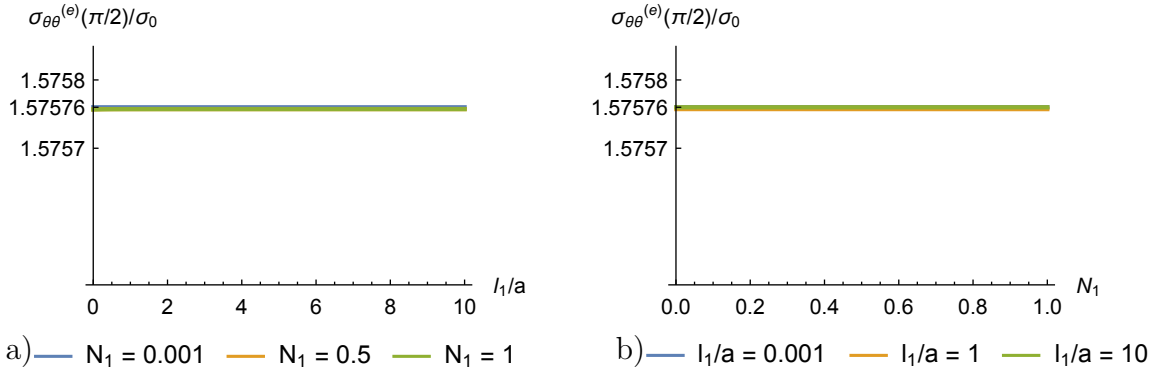

Figure 8: Stress concentration factor $\sigma_{\theta\theta}^{(e)}(\pi/2)$ for $g = 0.5$, $\nu_1 = 0.25$, $\nu_2 = 1/3$, $N_2 = 0.001$, $\ell_2/a = 0.001$ and a) various values of N_1 as function of ℓ_1/a, b) various values of ℓ_1/a as function of N_1.

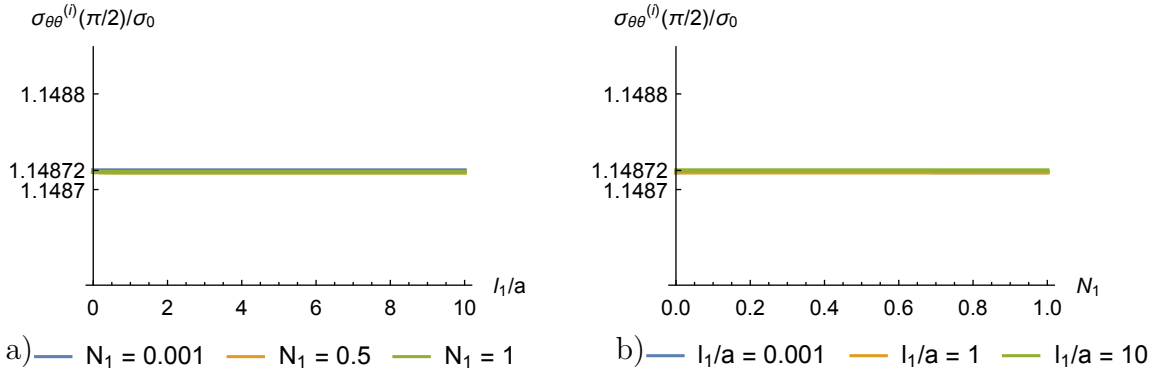

Figure 9: Stress concentration factor $\sigma_{\theta\theta}^{(i)}(\pi/2)$ for $g = 2$, $\nu_1 = 0.25$, $\nu_2 = 1/3$, $N_2 = 0.001$, $\ell_2/a = 0.001$ and a) various values of N_1 as function of ℓ_1/a, b) various values of ℓ_1/a as function of N_1.

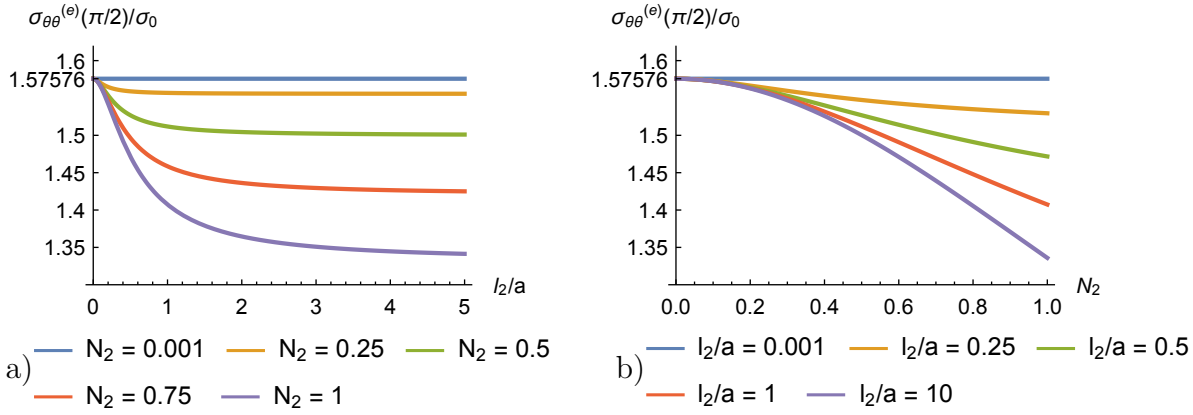

Figure 10: Stress concentration factor $\sigma_{\theta\theta}^{(e)}(\pi/2)$ for $g = 0.5$, $\nu_1 = 0.25$, $\nu_2 = 1/3$, $N_1 = 0.001$, $\ell_1/a = 0.001$ and a) various values of N_2 as function of ℓ_2/a, b) various values of ℓ_2/a as function of N_2.

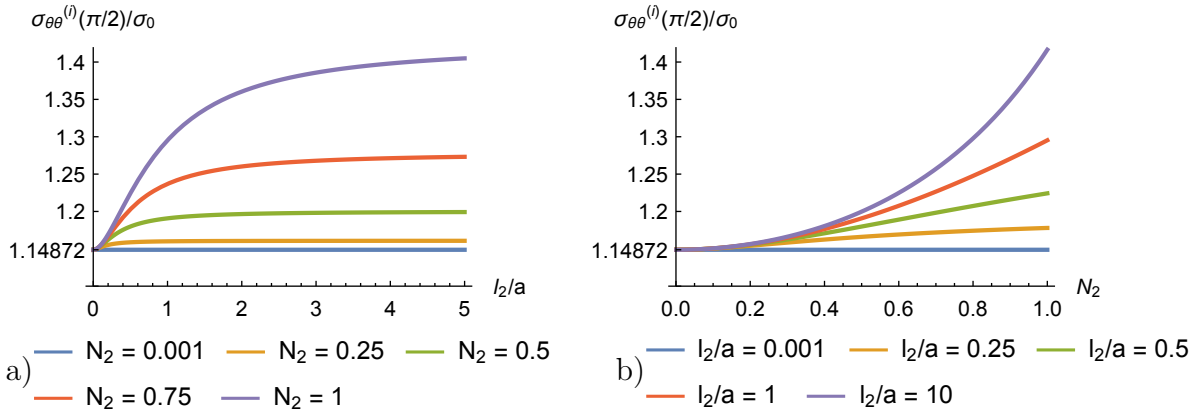

Figure 11: Stress concentration factor $\sigma_{\theta\theta}^{(i)}(\pi/2)$ for $g = 2$, $\nu_1 = 0.25$, $\nu_2 = 1/3$, $N_1 = 0.001$, $\ell_1/a = 0.001$ and a) various values of N_2 as function of ℓ_2/a, b) various values of ℓ_2/a as function of N_2.

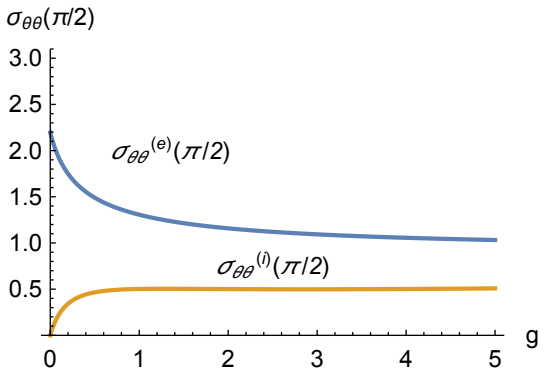

a) $h_r = 0$, $h_\theta = 1$

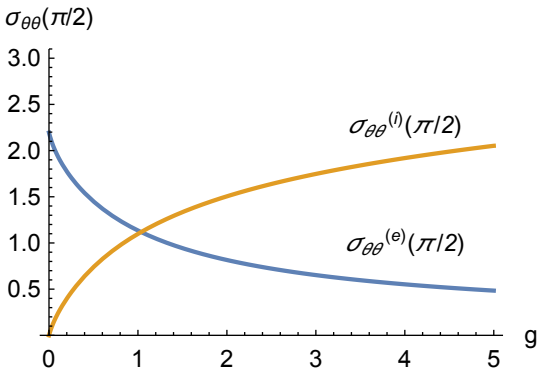

b) $h_r = 1$, $h_\theta = 0$

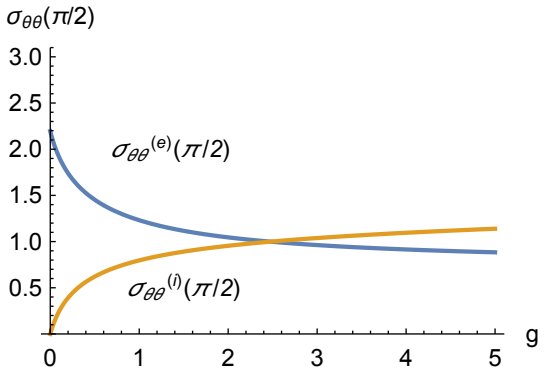

c) $h_r = h_\theta = 0.25$

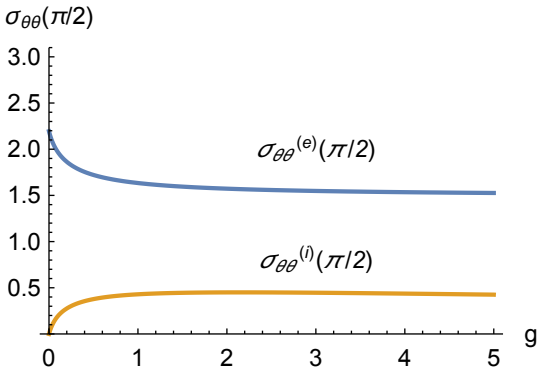

d) $h_r = h_\theta = 1$

Figure 12: $\sigma_{\theta\theta}^{(e)}(\pi/2)$, $\sigma_{\theta\theta}^{(i)}(\pi/2)$ for $\nu_1 = 0.35$, $\nu_2 = 0.25$, $N_1 = 0.75$, $N_2 = 0.9$, $\ell_1/a = 0.1$, $\ell_2/a = 0.75$ and various values of h_r, h_θ and $h_\phi = 0.1$ as function of g.

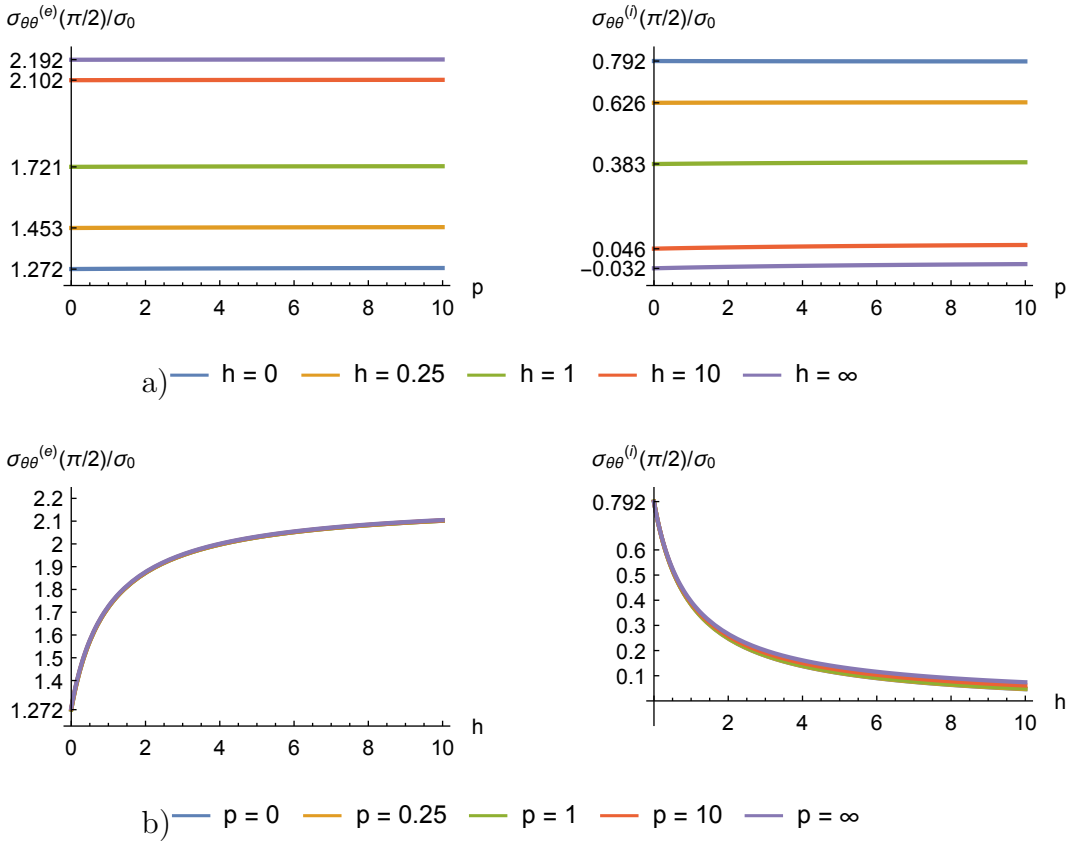

Figure 13: A "softer" inclusion, $g = 0.5$: $\sigma^{(e)}_{\theta\theta}(\pi/2)$, $\sigma^{(i)}_{\theta\theta}(\pi/2)$ for $\nu_1 = 0.35$, $\nu_2 = 0.25$, $N_1 = 0.75$, $N_2 = 0.9$, $\ell_1/a = 0.1$, $\ell_2/a = 0.75$ as functions of $h = h_r = h_\theta$ and $p = h_\phi$.

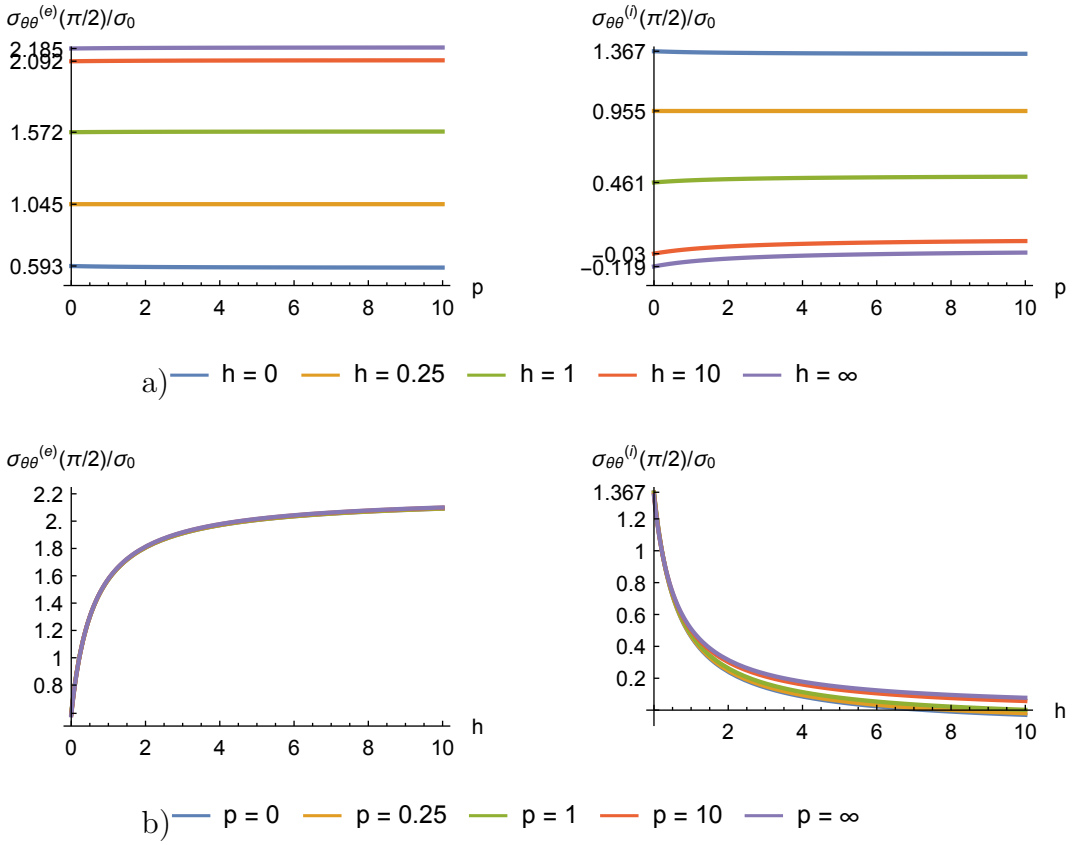

Figure 14: A "stiffer" inclusion, $g = 2$: $\sigma_{\theta\theta}^{(e)}(\pi/2)$, $\sigma_{\theta\theta}^{(i)}(\pi/2)$ for $\nu_1 = 0.35$, $\nu_2 = 0.25$, $N_1 = 0.75$, $N_2 = 0.9$, $\ell_1/a = 0.1$, $\ell_2/a = 0.75$ as functions of $h = h_r = h_\theta$ and $p = h_\phi$.

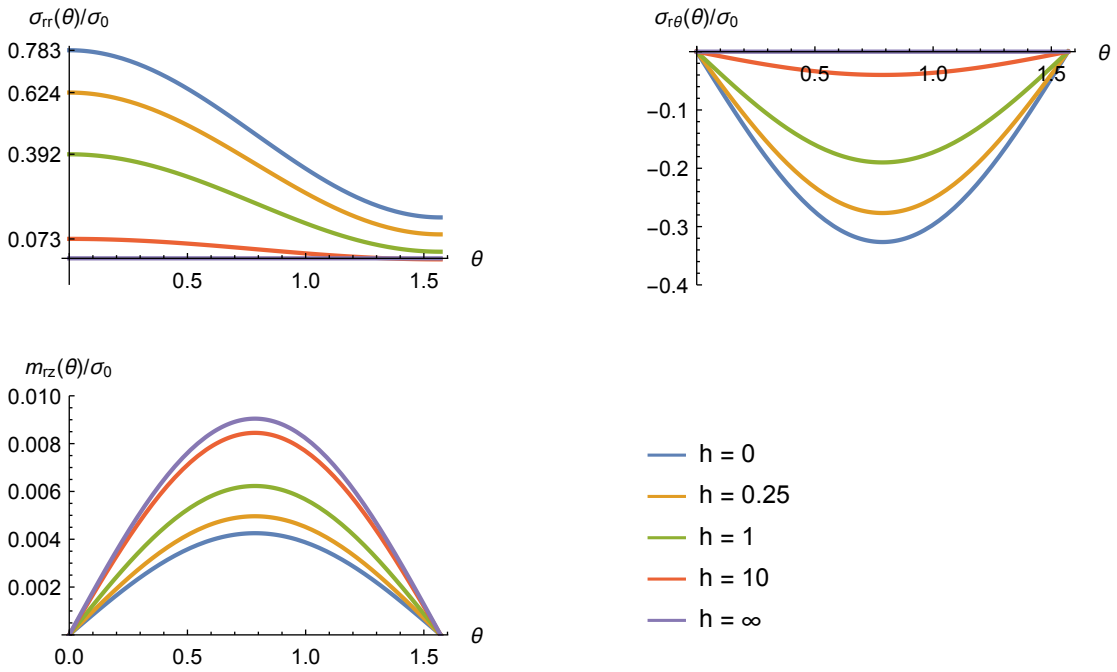

Figure 15: A "softer" inclusion, $g = 0.5$: distribution of σ_{rr} for $\nu_1 = 0.35$, $\nu_2 = 0.25$, $N_1 = 0.75$, $N_2 = 0.9$, $\ell_1/a = 0.1$, $\ell_2/a = 0.75$, $g = 0.5$ for various values of h and $p = 1.0$.

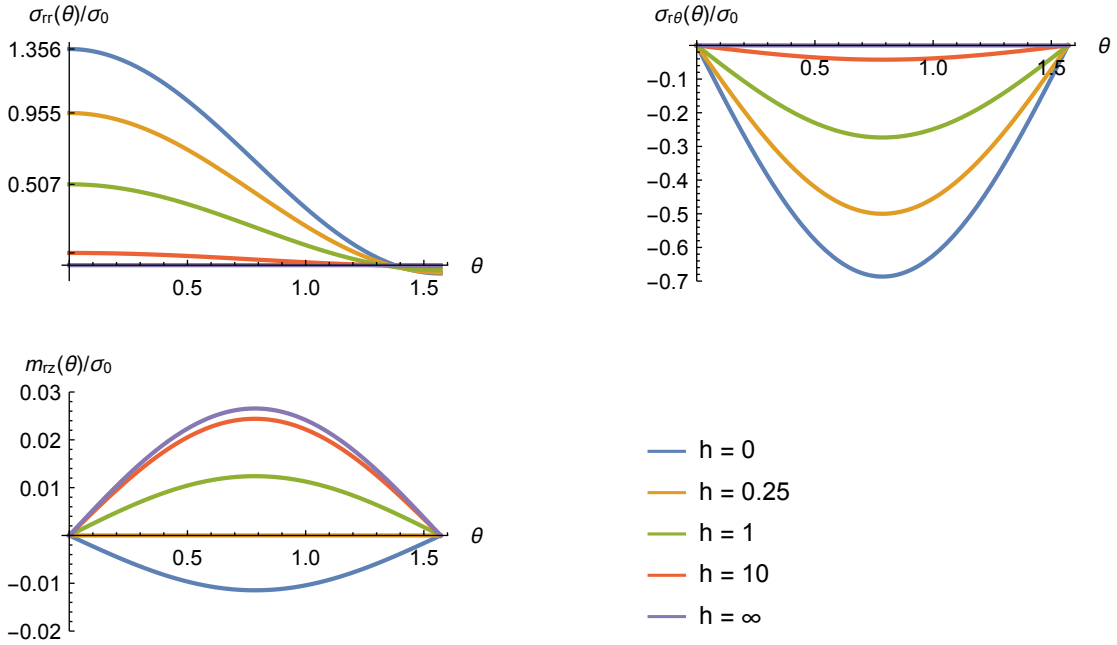

Figure 16: A "stiffer" inclusion, $g = 2$: distribution of σ_{rr} for $\nu_1 = 0.35$, $\nu_2 = 0.25$, $N_1 = 0.75$, $N_2 = 0.9$, $\ell_1/a = 0.1$, $\ell_2/a = 0.75$, $g = 0.5$ for various values of h and $p = 1.0$.

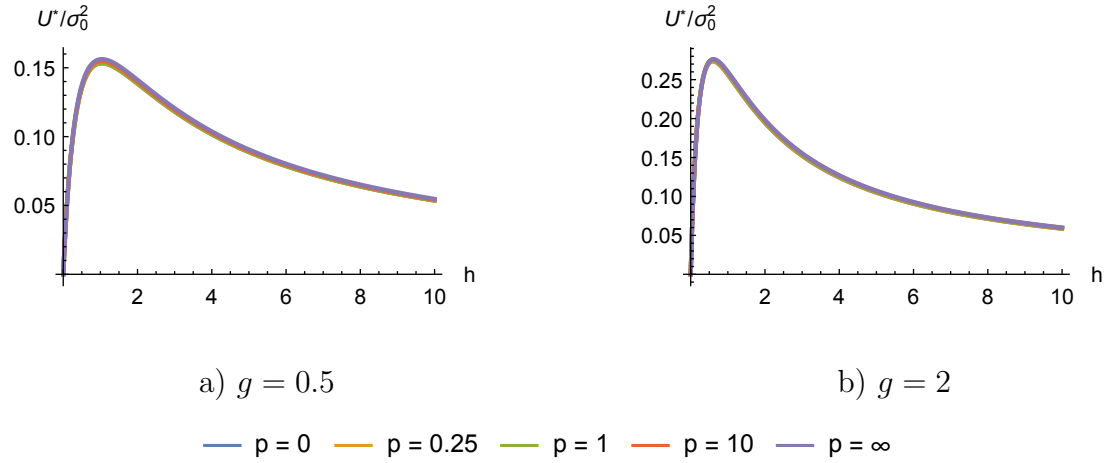

Figure 17: Maximum values of the normalized interface energy density function $U^\star = U(0)$ as function of $h = h_r = h_\theta$ for various values of $p = h_\phi$. Material parameters are set to $\nu_1 = 0.35$, $l_1/a = 0.1$, $N_1 = 0.75$, $\nu_2 = 0.25$, $l_2/a = 0.75$, $N_2 = 0.9$.